Study on a liquid cooled battery thermal management system pertaining to the transient regime

Yuqi Huang[a,b,c], Shun Wang[a], Yiji Lu [a,d,*], Rui Huang[a,c], Xiaoli Yu[a,c]

[a] Department of Energy Engineering, Zhejiang University, Hangzhou, 310027, Zhejiang, China

[b] State Key Laboratory of Clean Energy Utilization, Department of Energy Engineering, Zhejiang University, Zheda Road 38, Hangzhou, 310027, China

[c] Ningbo Research Institute, Zhejiang University, Ningbo, 315100, China

[d] Durham Energy Institute, Durham University, Durham, DH1 3LE, United Kingdom

Abstract

The research on battery thermal management systems in a transient and ultimate perspective is important to maintain the battery temperature within a reasonable range and save energy. In the present study, the transient and ultimate behaviors in a battery module consisting of 48 cells cooled by liquid are considered as the main focus. A lumped mass model with cold plate cooling design is developed to simulate battery module cooling performance. The results suggest that there is a cooling cap upper limit for a cold plate cooling system. When the inlet mass flow rate of the cold plate reaches a certain range, the cooling effect will not be improved obviously any more. The optimal Reynolds number for the designed cold plate and module is 475. In addition, there is a cooling hysteresis time for the indirect cooling structure. When the inlet flow rate increases suddenly, the surface temperature of the cells does not immediately decrease. For example, even with the discharge rate is 1C, the delay time is up to 66.37 s. Therefore, when considering precise control strategies of a battery thermal management system, the dynamic empirical correlations proposed by this study can offer some useful guidance.

Keywords: Cylindrical Lithium-ion Battery; Thermal Management; Indirect Liquid Cooling; Cooling Capacity; Hysteresis Time

Nomenclature

Abbreviations

BTMS	battery thermal management system
CFD	computational fluid dynamics
EMF	electro motive force
EV	electric vehicle
FLC	fuzzy logic control
ROM	reduced-order model
SOC	state of charge
UDF	user defined function

Subscripts

a	ambient
avg	average
d	delay
hes	heat exchange surface
i	inlet
w	water

Greek letters

ρ	density, $kg•m^{-3}$
ν	kinematic viscosity, m^2/s
λ	thermal conductivity, w/(m•K)
φ	heat generating rate per unit of time and volume, W/m^3

Symbols

C_p	specific heat capacity, $J•kg^{-1}K^{-1}$
d	equivalent diameter, m
D	discharge rate, C
E	open-circuit voltage, V
h	convective heat transfer coefficient, $W•m^{-2}\ K^{-1}$
I	current through the battery, A
k	thermal conductivity, $W•m^{-1}K^{-1}$
Nu	Nusselt number
P	pressure, pa
q	heat flux, $W•m^{-2}$
Q	mass flow rate, kg/s
R	battery internal resistance, Ω
Re	Reynolds number
t	time, s
T	temperature, K
U	inlet velocity magnitude, m/s
$\vec{v}$	velocity, m/s
V_b	effective calculated volume of the individual battery cell, m^3

1.Introduction

Battery thermal management system (BTMS) is an important and efficient facility to maintain the battery temperature within a reasonable range, thereby avoiding energy waste and battery thermal runaway [1]. The liquid cooling systems, with the advantage of high efficiently, low cost, and easy to combine with other cooling component, have been adopted by many leading EV manufactures (e.g., Chevrolet Volt, Tesla Model 3 and Model S, BMW i3 and i8) [2]. The coolant, usually ethylene glycol water, of an indirect cooling system has a much lower viscosity than the dielectric mineral oil usually used for direct liquid cooling. In the case of the same power consumption, the indirect cooling system can achieve a larger fluid flow rate [3].

Therefore, in the field of vehicle BTMS, indirect-contact liquid cooling systems have been extensively studied by passing the liquid through a channel, which can be a metal plate with built-in channels (cold plate) or flat tube [4].

In the liquid cooling system, the influences by inlet mass flow rates or coolant temperature at different discharge rates are important characteristics for battery module. It has been studied broadly [5, 6], and quantitative parameters are given as optimal values for specific liquid cooling system configurations. Wang at el. [7] proposed an orthogonal test to figure out the influence of inlet velocity and geometry parameters on cooling performance with curved surface pipes, and this test demonstrated that when the inlet velocity ranged from 0.2~0.5 m/s and channel numbers ranged from 1~2 the liquid cooling system achieved an improved performance. Huo et al. [8] investigated the influence of channel parameters and inlet mass flow rates on the cooling effect. This study showed that when the inlet mass flow rate got larger, the cooling performance was always got improved, but a smaller increasing trend was found. And the recommended optimal inlet flow rate was found to be 5×10^{-4} kg/s. Deng et al. [5] studied the effects of inlet mass flow, channel and cold plate arrangements on thermal performance using a battery pack cooling system with four modules and five cold plates, and proposed that 1×10^{-3} kg/s was suitable for the whole battery pack mass flow inlet with 3C and 5C discharge. Tang et al. [9] conducted an experiment on three different water cooling strategies with mini-channel cold plat, the results showed that flow rates and discharge rates were important influence factors on maximum temperature, and a 3.3×10^{-2} kg/s inlet flow rate was selected as an optimal value for temperature uniformity. Ozge and Tahir [10] numerical simulated a battery pack, and noticed the temperature of batteries lowered with the decreasing of charge ratio, but

this process required a long time. In most of these studies, both the inlet flow rate and discharge rate were controlled to be stable on each simulating or testing case. This way of processing can simplify the analyzation, and help to conclude the most ideal combinations of conditions. But it was definitely unlike the real working process, in which the flow and discharging rates would be varied according to different driving requirements and environment conditions frequently.

For electric or hybrid electric vehicles, the scope of thermal management system includes not only cooling or heating the batteries, but also cooling the electric machinery, machine controller, condenser, and other driven parts. To handle these operations, it needs a complicated control system with optimal control strategy and fast response [11]. Hamut et al. [12] optimized the thermal management system of a hybrid electric vehicle by single and multi-objective evolutionary algorithms, achieved a 13% higher exergy efficiency and 5% lower environmental impact at the expense of a 27% increase in the total cost. Gao et al. [13] investigated the thermal management by employing fuzzy logic control (FLC). They proposed the reduced-order model (ROM) of a battery pack whose heat transfer coefficient varied with coolant flow velocity, verified the accuracy of ROM by CFD study, then validate the effectiveness of FLC by ANSYS and MATLAB co-simulation. Liu and Zhang [14] developed an intelligent air-cooling battery thermal management via neural network-based model predictive control. They carried a large number of transient fluid dynamics simulations prior to building the control models. The CFD simulations not only helped to pre-optimizing the structure, but also contributed to the prediction of real-time battery temperature. Their studies showed a 15.8% energy efficiency improvement by employing model predictive control. It is worthwhile to devote more attention to this issue because unnecessary wastage of energy could be reduced using model predictive

control [15]. To the demand of a high-performance precise control strategy in vehicle BTMS nowadays, the research on the transient thermal behaviors of the lithium-ion battery module at different cooling and discharge conditions, which decide the response time in the control system, is essential and important. Also, the instant heat release and heat fluctuations at extreme discharge conditions could be a strenuous test, requiring the thermal management system to have both good heat dissipation performance and rapid response capability, especially when the battery module may face the problem of battery thermal runaway, which could bring potential safety hazards to the passengers. So it is crucial to determine the ultimate cooling capacity of the BTMS. However, most of the research efforts about BTMS now are focused on either cooling technology creation [16], system optimization [17], material and structures innovation [18], or steady performance evaluation [19].

In order to fill this gap, a typical battery module including battery cells and cold plates is taken as the object to deeply investigate the transient and ultimate thermal behaviours under various control commands in present study. The battery heat generation is calculated by transient lumped mass model, and the numerical method is validated by experiments. Cooling performance and temperature distribution were investigated with mass flow rates varying from 0 to 0.008 kg/s and discharge rates varying from 1C to 5C. Meanwhile, discharge rate, dimensionless flow parameter Reynolds number and dimensionless heat transfer coefficient Nusselt number are also investigated in order to find their inner relationship of a battery module with basic cold plate liquid cooling. For the transient response, the relationship between the liquid cooling hysteresis time and the discharge rate is also identified and studied. Finally,

empirical correlations are proposed to offer guidance and directions regarding the design and control of similar battery module liquid cooling systems.

This research aims to reveal the temperature changing rules of the battery module under various control conditions. Other than the study on cooling effect, a parameter named as hysteresis time, which is proposed to evaluate the rapidness of cooling system response after a sudden change, is used to potentially address the research gap in the comprehensive study of heat dissipation performance and response capability. In addition, the battery module liquid cooling system is studied from the perspective of precise control and ultimate performance analysis. The organic combination of the two aspects can bring a better battery thermal management scheme, which is the innovation point of the present study.

2.Experimental method

A single module which consists of 48 18650-type cylindrical batteries is selected as the experimental object, as shown in Fig. 1(a). A cooling plate is placed on each side of the module to test the temperature response of the battery module under liquid cooling conditions, and the finalised arrangement is shown in Fig. 1(b). The thermocouple probe penetrates into the interior of the battery module. The specific measuring point distribution is shown in Fig. 1(c), and there are 11 representative and dispersed thermocouple temperature measuring points in total. It is important to note that every thermocouple is arranged in the middle of the battery cylindrical surface for comparison.

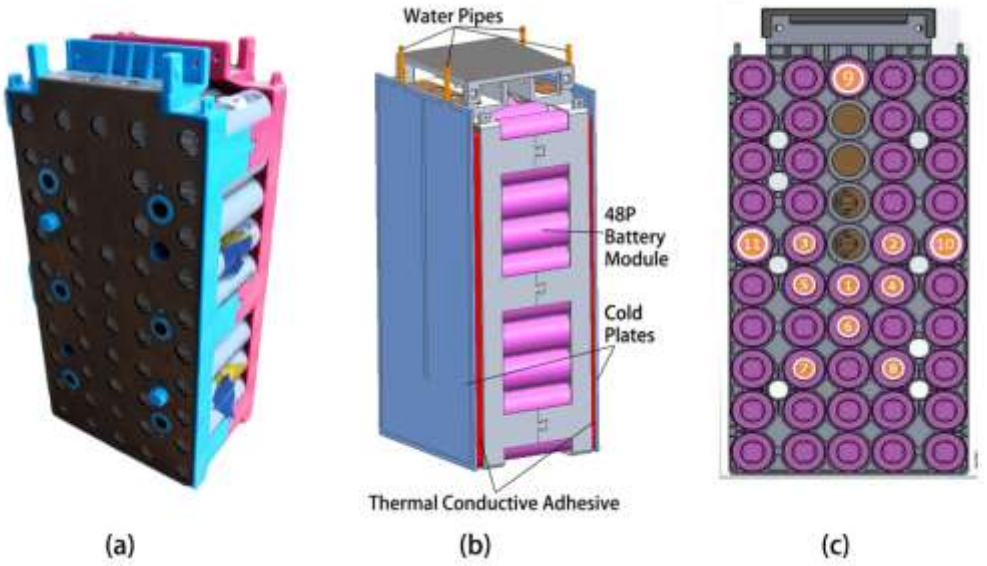

Fig. 1 Experiment test object and internal temperature measurement point distribution, (a) Battery module (b) Arrangement of cold plates relative to the battery module (c)Thermocouple distribution points

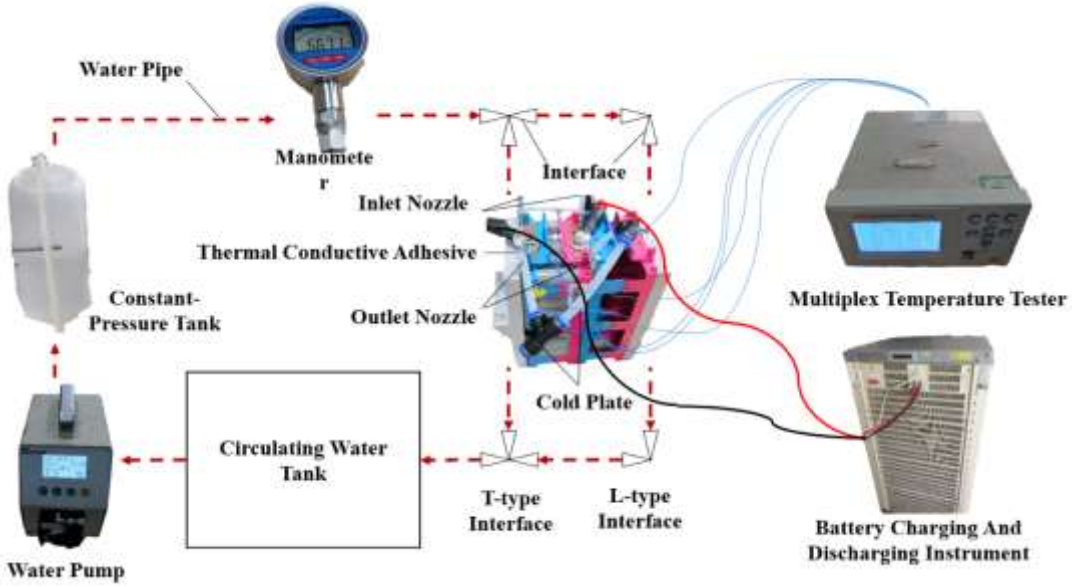

Fig. 2 48P liquid cooling module temperature characteristic test bench

Fig. 2 shows a schematic of the entire. The water in the circulating water tank is pumped by the water pump and then passes through the stabilized water tank in order to obtain a pressure-stable water flow. Through the shunting of the T-type or L-type interface, the water flow enters the cold plates on both sides of the battery module uniformly. After the cooling process is completed, the water flow is collected into the circulating water tank through the interface to

complete the entire cycle. In this process, the battery charging and discharging instrument charges or discharges the battery module, and the multi-channel temperature tester is responsible for recording the temperature data of each thermocouple.

In this experiment, two different cases, including the natural convection and the liquid cooling with the total flow of 144 mL/min, are tested at a 1.5 C discharge rate to obtain the change rules of the battery module cell surface temperature under different cooling conditions. The experimental results will be summarized together with the results of the simulation in Section 3.4.

3.Simulation models and verification

3.1 Lithium battery heat generation simulation method

In the discharging process, the battery temperature would also be raised in a nonlinear trend for the nonlinear heat generation. The heat generating rate of single cell during discharging can be calculated using Bernadi equation [20] as shown in Eq. (1), where φ (W/m^3) represents battery heat generating rate per unit of time and volume; I (A) is the current through the battery, which is positive when charging and negative when discharging; V_b (m^3) is the effective calculated volume of the individual battery cell; R is the total resistance; E (V) is the tested voltage and open-circuit voltage of the battery cell; T (K) is the battery temperature in the current; and dE/dT is a parameter related to the electrochemical reaction named the ElectroMotive Force (EMF) temperature coefficient.

$$\varphi = \frac{1}{V_b}\left[I^2R + IT\frac{dE}{dT}\right] \quad \text{Eq. (1)}$$

Battery internal resistance R and EMF temperature coefficient $\frac{dE}{dT}$ can be obtained through experimental measurements and fitting. The fitting method of the experimental results

in this study is described in detail by Eq. (2) and Eq. (3), and battery State of Charge (SOC) is simplified to be linearly related to charge/discharge time. The corresponding Coefficient P_{ij} of the internal resistance R values at 1.5C discharge rate are listed in Table 1, and the corresponding coefficient a_k of $\frac{dE}{dT}$ are listed in Table 2.

$$R = \frac{Z_0+A_{01}\cdot soc+B_{01}\cdot T+B_{02}\cdot T^2+B_{03}\cdot T^3}{1+A_1\cdot SOC+A_2\cdot SOC^2+A_3\cdot SOC^3+B_1\cdot T+B_2\cdot T^2} \quad \text{Eq. (2)}$$

$$\frac{dE}{dT} = \sum_{k=0}^{n=5} a_k SOC^{5-k} \quad \text{Eq. (3)}$$

Table 1 Coefficient of battery internal resistance R

Coefficient	Reference value	Coefficient	Reference value
z_0	141.19581	A_1	−1.1684
A_{01}	-20.66884	A_2	3.7948
B_{01}	-4.16739	A_3	−4.18158
B_{02}	0.09886	B_1	0.00993
B_{03}	-7.21187E-4	B_2	2.65693E-4

Table 2 The coefficient a_k of dE/dT

Coefficient	a_0	a_1	a_2	a_3	a_4	a_5
Reference value	42.969	-102.6	75.156	-8.2708	-9.75	2.74

In general, the heat generation simulation method of lithium batteries can be summarized as follow:

STEP 1: Obtain the corresponding points of internal resistance R (with Temperature T and SOC) and EMF temperature coefficient $\frac{dE}{dT}$ (with SOC) through experimentation.

STEP 2: Fit the data points measured by experimentation and export continuous expressions using suitable fitting methods such as polynomial or rational function.

STEP 3: Prepare heat-generating correlation and UDFs through Eq. (1) by fitting results

and associate the heat producing zone with the battery core zone.

3.2 Control equations

According to the theory of heat transfer, a convective boundary condition exists at each of the battery's outer walls. Newton's Law of Cooling suggests that the amount of heat dissipated due to the movement of a fluid can be determined using Eq. (4), where T_a (K) is the ambient temperature, and h_a ($W \cdot m^{-2} K^{-1}$) is the convective heat transfer coefficient of fluid.

$$q_a = h_a(T_b - T_a) \quad \text{Eq. (4)}$$

The heat transfer fluid, water, was used as cooling medium. The energy conservation equations for the liquid within the cold plate channels are calculated using Eq. (5), where ρ_w ($kg \cdot m^{-3}$), C_{pw} ($J \cdot kg^{-1}K^{-1}$) and k_w ($W \cdot m^{-1}K^{-1}$) are the density, heat capacity and thermal conductivity of the liquid, respectively. T_w (K) is the liquid temperature, and $\vec{v}$ ($m \cdot s^{-1}$) is the velocity of the liquid.

$$\frac{\partial(\rho_w c_{pw} T_w)}{\partial t} + \nabla \cdot \left(\rho_w c_{pw} \vec{v} T_w\right) = \nabla \cdot (K_w \nabla T_w) \quad \text{Eq. (5)}$$

The mass and momentum conservation equations can be written as the following two equations, where P (Pa) is the static pressure.

$$\frac{\partial \rho_w}{\partial t} + \nabla \cdot (\rho_w \vec{v}) = 0 \quad \text{Eq. (6)}$$

$$\frac{\partial(\rho_w \vec{v})}{\partial t} + \nabla \cdot \frac{\partial(\rho_w \vec{v}\vec{v})}{\partial t} = -\nabla P \quad \text{Eq. (7)}$$

3.3 Simulation geometry and boundary conditions

The overall schematic drawing of a module is shown in Fig. 3. The module is composed of two half-cells (18×32.5 mm) on the top and bottom, and a cold plate sandwiched between two half-cells. In the experiment, the module has batteries containing 48 cells and the same arrangement as in Fig. 3. The upper and lower sides of the module are set to a symmetry plane

to ensure that the simulation results of a single module are representative. The inlet and outlet are placed on one side of the cold plate as illustrated in Fig. 3(a). Any end surface of the half-cell is in direct contact with the cold plate surface, and the surrounding area is filled with air.

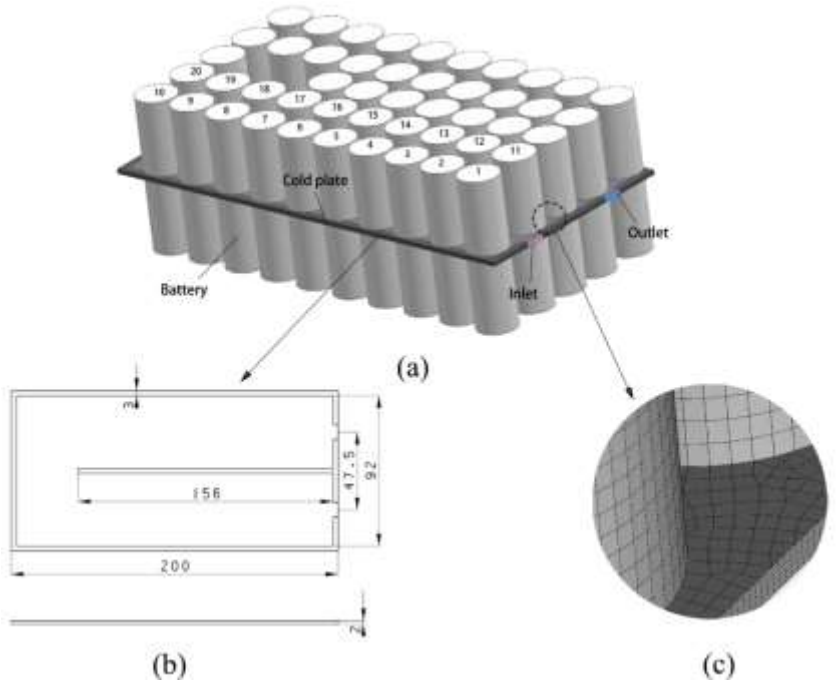

Fig. 3 Schematic drawing of a module, (a) Cold plate and battery cells arrangement (b) cold plate model geometry (c) grid detail at battery cells and cold plate interface

The geometric information of the cold plate in this designed cooling system structure is shown in Fig. 3(b). In particular, the internal flow of the cold plate is designed as a mini channel structure. The thickness of the cold plate was 2 mm, and the flow channel was 1 mm. The grid detail at battery cells and cold plate interface is shown in Fig. 3(c), and a hexahedron mesh is adopted to improve calculation accuracy and reduce the number of total grids. The total grid number of the module is approximately 1.4 million and the minimum mesh size is 0.25 mm near the cold plate inlet and outlet.

The mass flow rates of the inlet are 0, 0.0001, 0.00025, 0.0005, 0.001, 0.002, 0.004 and 0.008 kg/s, respectively. The outlet is set as outflow condition to guarantee convergence. The outer surfaces, except for the symmetry plane, are set to the third boundary condition. Since

this is natural convection, the convective heat transfer coefficient could take an empirical value of 5 W/(m^2•K). Due to the small mass flow, the Reynolds numbers involved in this model are all less than 2300. Therefore, a laminar flow viscous model is applied. The pressure-based solver was selected, and the pressure discretization scheme is SIMPLEC. The physical parameters involved in this module are also shown in Table 3.

Table 3 Physical parameters involved in the module

Zone name	Material property parameter		
	Density kg/m^3	Thermal conductivity W/(m•K)	Specific heat capacity J/(kg•K)
BATTERY CORE	1924.1	Radial 1.81 Axial 2.51 Circumference 2.51	1264.97
AIR	1.29	0.0242	1006.43
WATER	998.2	0.6	4182
ALUMINIUM	2719	202.4	871

The thermal conductivity coefficients of the wall on the negative side, the wall on the positive side and the wall forming the cylinder surface are 100, 100 and 52.84 W/(m•K), respectively. For this, there is one shell conduction layer with a thickness of 2 mm. The time step size was set at 4 s. The total calculation time were 2880, 1440, 960, 720, 576 seconds corresponding to the 1~5 C discharge rates. The initial and environmental temperature is 288 K, and the other settings remain at default level.

3.4 Simulation method verification

In our previous study [21], the simulation method was used to simulate single 18650 battery surface temperature variations at different discharge rates as shown in Fig. 4. The experiment and simulation fits well with a maximum error of 1.73 ℃.

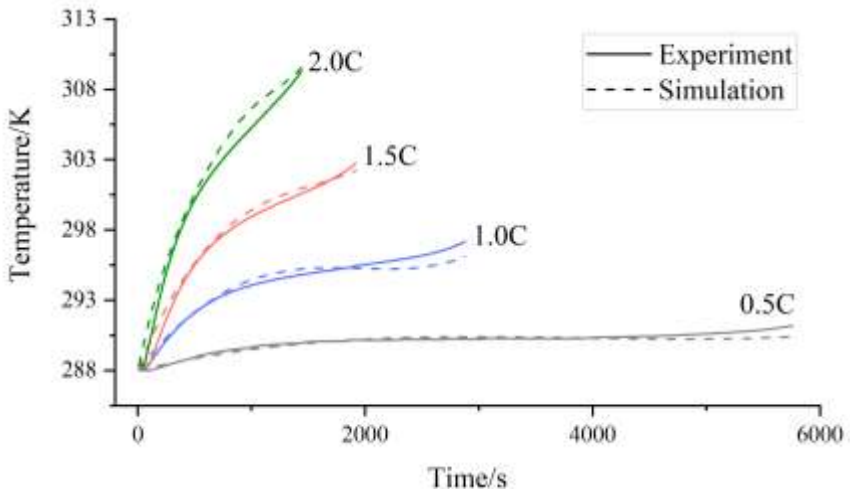

Fig. 4 Temperature comparison of experimental and simulation results at single battery surface

The temperature differences of the module at some thermocouple distribution points and their maximum relative deviation at 1.5C discharge is shown in Fig. 5. The temperature error at module scale is larger than the results for a single battery due to model simplification such as simplified treatments of the contact thermal resistance and the plastic shell, but the maximum relative deviation is less than 8%. The results of the experiment and simulation are within reasonable deviations, so the simulation method is considered to be reliable.

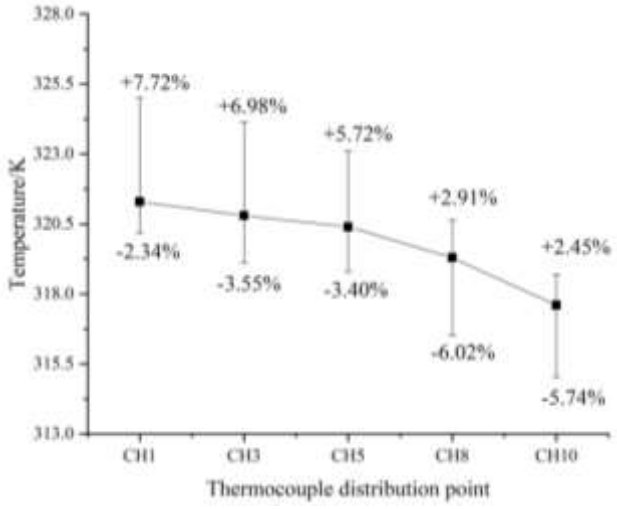

Fig. 5 Temperature differences at some thermocouple distribution points and their maximum relative deviation

4.Results and Discussion

4.1 Ultimate cooling capacity

The average surface temperature of batteries at 2C discharge is shown in Fig. 6. The graph shows that as the inlet mass flow rate increases, the average temperature curve of the cell surface gradually flattens. Therefore, the cooling system in the module can efficiently reduce the average temperature of the cell surface throughout the whole discharge process. As the mass flow rate of the inlet increases, the average surface temperature of the battery cells gradually decreases with a same discharge duration, but the magnitude of the decrease gradually slows down. That preliminary means there may be a cooling capacity limit for the system. In order to demonstrate the regular pattern more clearly, more concrete data under different discharge conditions (1C-5C) at the end of discharge (at SOC=20%) are given in Fig. 9 and will be analysed later.

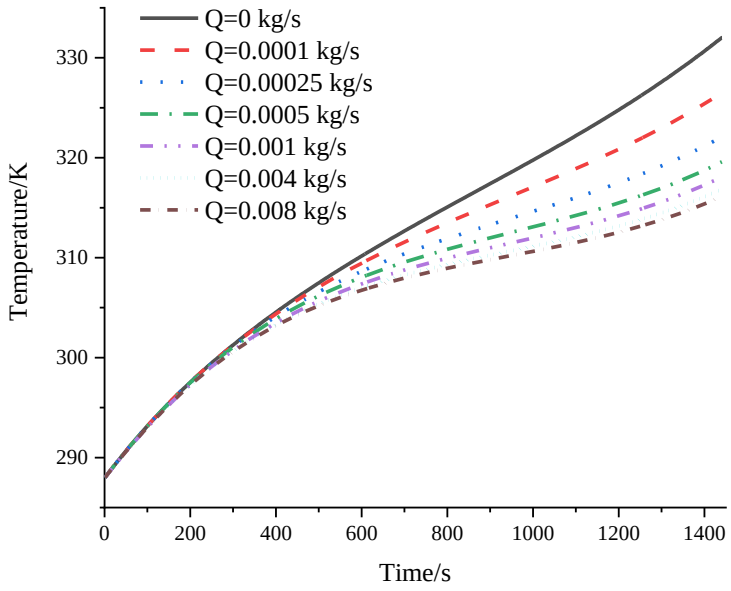

Fig. 6 Average surface temperature of batteries at 2C discharge

The Reynolds number based on the inlet equivalent diameter is defined by Eq. (8), and it is used to represent the dimensionless inlet flow rate to make the conclusions of the study more

general, where $U_{i,avg}$ (m/s) is the inlet average velocity, d_i (m) is the inlet equivalent diameter, and ν (m^2/s) is the kinematic viscosity of the fluid.

$$\mathrm{Re} = \frac{U_{i,avg} \cdot d_i}{\nu} \qquad \text{Eq. (8)}$$

The contour of temperature distribution in the middle section of the cold plate is shown in Fig. 7. Under the discharge rate of 2C, when the Reynolds number is 118 or even 237, the cooling water of the sections is relatively overheated particularly at the outlet side. Conversely, when the Reynolds number is as high as 951, the temperature of the internal flow of the cold plate is almost the same as the inlet mass flow temperature (15 ℃), so there may be a huge waste of pump energy. More specifically, when the Reynolds number is 475, the temperature distribution is relatively uniform. Therefore, 475 is the optimal cold plate inlet Reynolds number for the designed simple and basic cooling system structure.

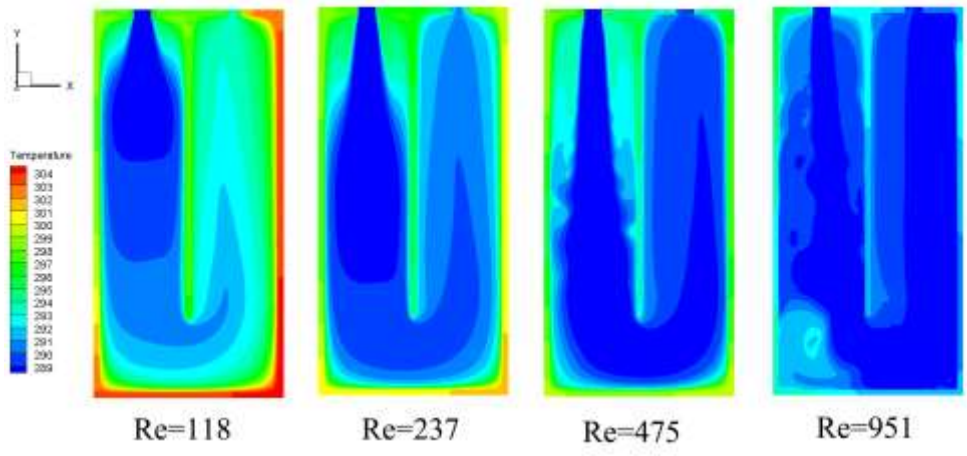

Fig. 7 Temperature contour of cold plate at 2 C discharge

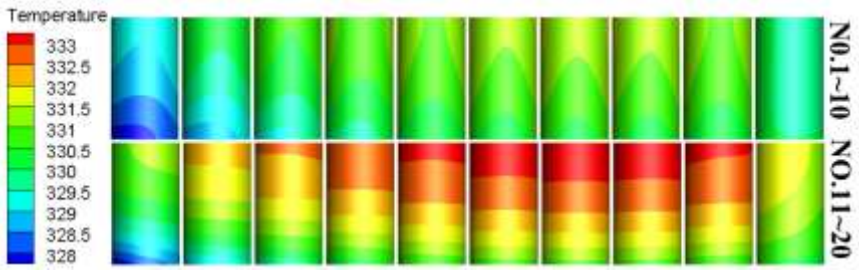

(a)

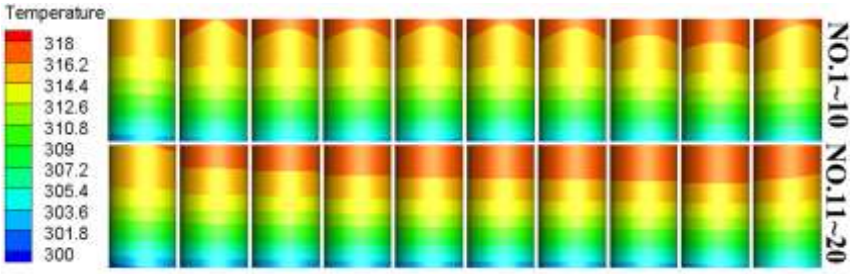

(b)

Fig. 8 Surface temperature contour of battery cells at 2C discharge rate. (a) Re=0; (b) Re=475.

Fig. 8 shows the surface temperature contours of battery cells at 2C discharge rate, Re=0 and Re=475, respectively. The number of each cell is shown in Fig. 3(a). The first row is numbered as No.1–10, and the second row is numbered as No. 11–20. According to the contours, when the Reynolds number is equal to 475, the maximum temperature is significantly lower than when the Reynolds number is equal to 0. Combined with Fig. 6, the design of the cooling system can reduce the surface temperature of the battery cells and maintain the temperature coherence of the core, which can substantially increase the service life of lithium batteries.

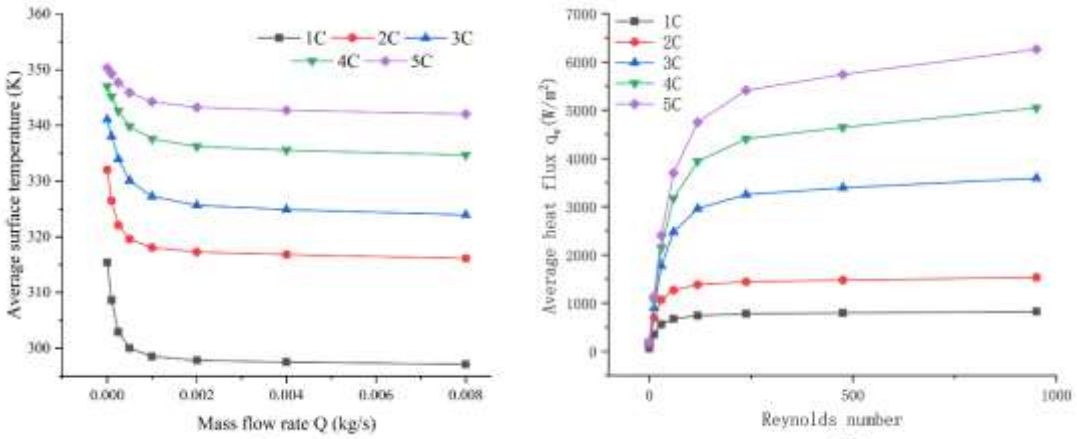

(a) **(b)**

Fig. 9 (a)The average surface temperature of batteries; (b) The average wall heat flux of cold plates at different discharge rate and mass flow rate

Fig. 9 display the average surface temperature of batteries and average wall heat flux of cold plate at different discharge rate and mass flow rate. Fig. 9(a) shows that when the discharge rate is low, increasing the mass flow rate from 0 will rapidly lower the surface temperature of

the batteries. When the discharge rate gets higher, the decrease in surface temperature of the batteries is becoming less obvious. However, the average heat flux q_w in Fig. 9(b) shows that when the discharge rate is higher, there will be a faster increase with Reynolds number increase from 0. It is because when the discharge rate is higher, the heat generation rate φ of the batteries increases nearly in square order of discharge rate from Eq. (1). So the heat exchange is greatly increased under the same mass flow rate, and so does the heat flux under the same heat transfer area. But with the cooling water being quickly heated, the surface temperature drop of the batteries will be smaller.

More importantly, as the inlet flow rate increases and when the inlet mass flow reaches a relatively high level, increasing the mass flow of the inlet barely improves the performance of the module liquid cooling system. This regular pattern occurs at no matter whether the discharge rates are high or low, and is more apparent at low discharge rates. This phenomenon may be caused by the following three reasons. First, the thermal resistance between the batteries and the cold water limits the heat transfer rate of the model, and this is the objective reason that limits the cooling capacity of this battery module cooling system. Second, from Fig. 7 it can be seen that when the Reynolds number increases, the average water temperature in the cold plate channel continue to approach the inlet water temperature. Compared to the rather high battery core temperature, it can be concluded that the temperature difference between the hot and cold ends has not increased significantly. The motive force of the heat transfer, represented by the temperature difference, only has tiny growth, so the cooling capacity gradually reaches the limit. Finally, when the discharge rate is low, the heat generated by the batteries is much less, so the cooling system approaches the cooling limit with relatively low inlet mass flow rate.

This phenomenon is called the Ultimate Cooling Capacity and is used for specific cold plate liquid cooling structure associated with the cooling of power batteries. Quantitatively, from the average surface temperature curves of battery cells and heat flux curves with inlet flow at each discharge rate, it is understood that the liquid cooling performance of the module is relatively superior when the inlet mass flow rate reaches 0.004 kg/s (Re=475), because continuing to increase the inlet mass flow will result in a significant increase in power consumption by water pump and will only achieve a slight improvement in performance of the system.

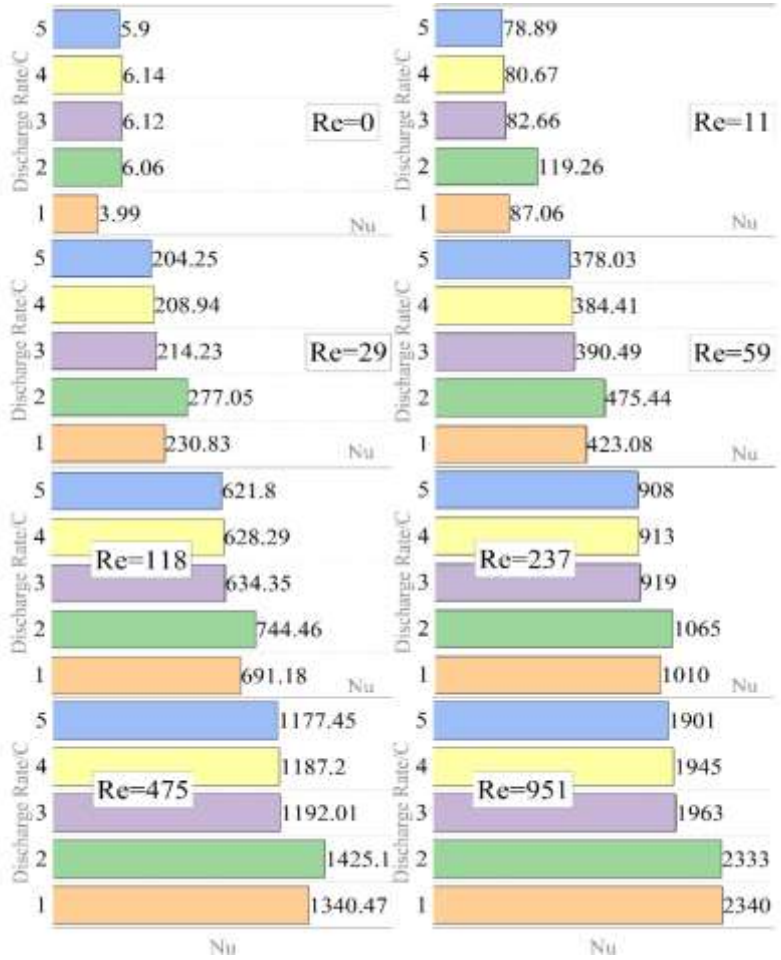

Fig. 10 Cold plate Nu number at different discharge rate and Reynolds number

Furthermore, the Nusselt number (Nu) is defined in Eq. (9) to characterize the convection strength between a moving fluid and a solid body, where h ($w/m^2 \cdot K$) is the surface heat transfer

coefficient of the water and the aluminium cold plate surface, and λ (w/m•K) is the thermal conductivity of the water.

$$\mathrm{Nu} = \frac{h \cdot d_{hes}}{\lambda} \qquad \text{Eq. (9)}$$

The Nusselt number at different discharge rate and Reynolds number in the water and cold plate surface is shown in Fig. 10. However, different to the average heat flux, the heat transfer strength continues to rise when discharge rates increase. That means the convection temperature difference between fluid and solid is reduced rapidly when the discharging rate increases because the convection strength and temperature difference are the two main factors impacting the wall heat flux according to Eq. (4). And with the Reynolds number varying, the 2C discharging rate condition always seems to achieve a relatively high Nu number, which indicates that the 2C discharging rate condition may be a more preferable working condition for the liquid cooling system because of its better heat transfer strength. However, for lithium-ion batteries, large rate charge and discharge could lead to reduced battery cycle life, which requires comprehensive choices.

4.2 Cooling hysteresis effect

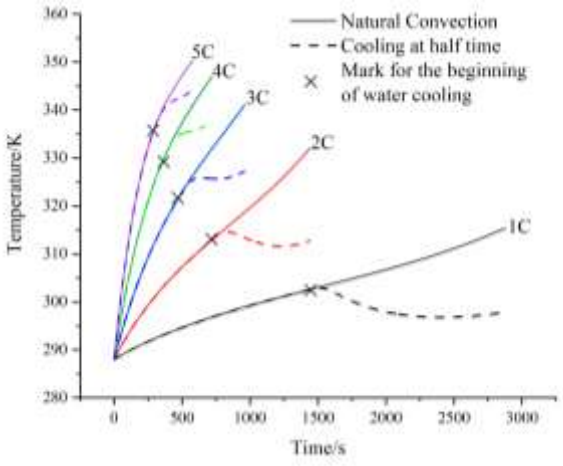

Fig. 11 Comparison of average surface temperature curves of battery cells between natural

convection cooling and water cooling at half time

Under different discharge rates (1C-5C), two sets of simulations were carried out and compared in Fig. 11. In the first set, the battery module was cooled by natural convection for the whole journey. However, in the other set, the module was cooled by natural convection for the first half of the discharge time and then it was cooled by water until discharge finished. This means that there was a sudden change in the inlet Reynolds number, from 0 to 475, which is the optimal cold plate inlet Reynolds number as previously discussed.

The black cross shown on Fig. 11 represents the exact time of circulating cooling water at each discharge rate. It can be observed that the temperature curves of water cooling are improved significantly compared to natural convection cooling, especially at low discharge rates. However, we find that it takes a certain amount of time from the beginning of liquid cooling system to significant temperature difference compared to air natural convection. In the current work, the significant temperature difference is set to 0.1 K below the temperature of natural convection, and this period of time is named the cooling hysteresis time t_d.

Based on the actual situation of the simulation model, the hysteresis time may be primarily attributed to two reasons. First, at the beginning of the process, it takes some time for the fresh water flow in the channel to circulate from the inlet to the outlet so that it could cool the battery cells gradually during this period of time. When the inlet mass flow rate is 0.004 kg/s (Re=475, the inlet velocity equals 0.22 m/s based on the inlet geometry), this period of time will take at least 1.42 seconds supposing that the flow chooses the shortest path to get through with no velocity loss. This period of time should account for quite a part of the total hysteresis time because more time is needed during the process than calculated due to the rapidly expanding flow channel cross section after the flow passing the inlet. Secondly, the thermal resistance

between the cold water and the high temperature batteries slows down the dissipating rate of the generated heat. Apart from the thermal resistance of the aluminium plate and the electrode material, the contact thermal resistance between them is considered to be the main thermal resistance. When the discharge rate D changes, due to the temperature field difference, the physical property parameters (such as thermal conductivity, etc.) of the materials used in this model change, and those materials have the property of thermal expansion and contraction. Those factors will make it difficult to determine the specific dynamic thermal resistance. In all, these two reasons result in the hysteresis time, and this would influence the accuracy of temperature prediction in system evaluation and controlling.

In order to quantitatively describe the difference in cooling hysteresis time at different discharge rates, the average surface temperature differences of battery cells ΔT under the two conditions (natural convection reduced by water cooling) are recorded in Fig. 12 from the exact time when circulation of cooling water commences. For 1-5C discharging rates, the corresponding cooling hysteresis time t_d are 66.37 s, 61.11 s, 58.07 s, 57.37 s and 57.41 s. The deviation between them is small, and the hysteresis time of each condition are about 60 s, showing a nonlinear change with different discharge rates.

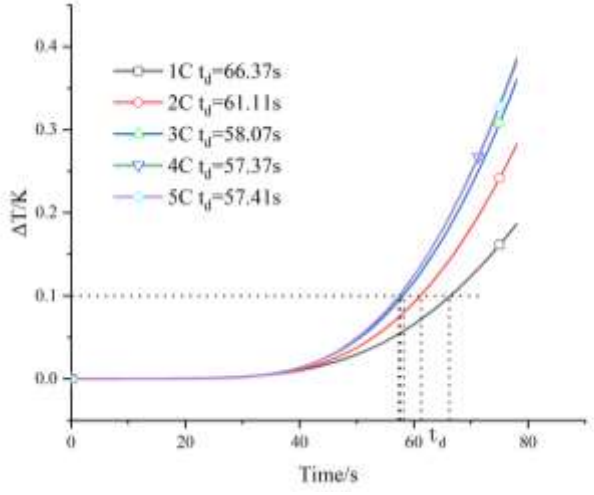

Fig. 12 The average surface temperature differences ΔT between natural convection and water cooling in different discharge conditions

4.3 Empirical correlations

By analysing data in Fig. 10, an empirical formula for the relationship between Nusselt number Nu and Reynolds number Re and discharge rate D is summarized in Eq. (10). The graph of the predicted values against the actual values is shown in Fig. 13. The R-square value is 0.90 with almost all the points being predicted with a ± 30% deviation, but when the Reynolds number is very low there may be a relatively large error. However, the correlation works well with a large range of Reynolds number, including the optimal Reynolds number discussed previously, and could offer some directions to similar battery module liquid cooling systems.

$$\mathrm{Nu} = -0.00232\mathrm{Re}^2 + 4.6\mathrm{Re} - 0.5\mathrm{D}^{1.5}\mathrm{Re}^{0.5} + 106 \qquad \text{Eq. (10)}$$

Also, an empirical formula between cooling hysteresis time t_d and discharge rate D is summarized as Eq. (11).

$$t_d = 12.11\mathrm{D}^{-0.939} + 54.32 \qquad \text{Eq. (11)}$$

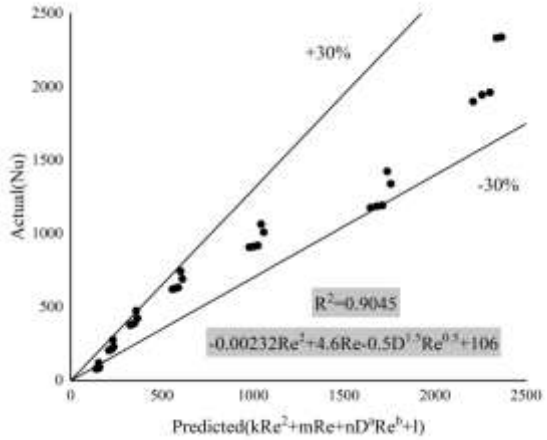

Fig. 13 Correlation of predicted vs. actual values

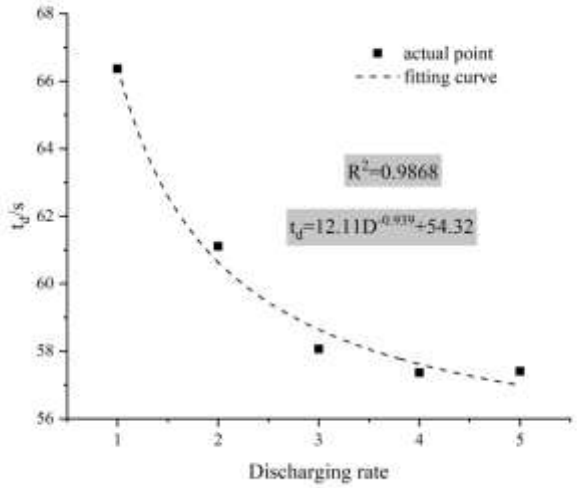

Fig. 14 Correlation curve between hysteresis time and discharge rate

The fitting curve is shown in Fig. 14 with actual points between hysteresis time and discharge rate. The R-square value is approximately 0.99 so that the correlation is quite accurate. From Fig. 14 it can be concluded that the lower the discharge rate, the larger the hysteresis time; at high discharge rates, especially at 4C and 5C discharge rates, the hysteresis time tends to be very similar. So, it is speculated that there is also a limit when the hysteresis time decreases as the discharge rate increases. In the dynamic control of the cooling system, the hysteresis time must be considered as contributing to the system response time. And Eq. (11) can offer some guidance for control systems to estimate hysteresis time and take actions in advance in similar liquid cooling systems so that the cooling effect will not be delayed.

5.Conclusions

In order to understand the transient and ultimate thermal behaviours of the battery module as controlled by water-cooled battery thermal management embedded system, the relationship between key parameters among discharge rate, dimensionless inlet flow rate and dimensionless heat transfer coefficient were studied in this paper. A lumped mass model was adopted for heat generation calculation of battery module with liquid cooling, and experiments were performed

to verify the modelling. Then the influence of cooling flow and discharge rate on cooling hysteresis time were discussed. The major conclusions are summarized as follows:

Increasing the inlet flow rate will cool the battery module more effectively but not efficiently. It is found that there is a reduction of cooling capacity per unit of inlet flow with an increasing inlet flow rate. In our current study, 475 is the recommended inlet Reynolds number for the simple and basic cold plate geometry, and an empirical correlation ($\mathrm{Nu} = -0.00232\mathrm{Re}^2 + 4.6\mathrm{Re} - 0.5\mathrm{D}^{1.5}\mathrm{Re}^{0.5} + 106$) is presented with an estimation of the convection Nusselt number by the Reynolds number and discharge rate with an error within ± 30%.

Moreover, with an abrupt change to the inlet flow, the cooling system's response time exhibits a hysteresis effect. The lower the discharge rates, the larger the hysteresis times. Particularly, when the discharging rate is 1C, the hysteresis time reaches 66.37 s. Also, a nonlinear empirical correlation ($\mathrm{t_d} = 12.11\mathrm{D}^{-0.939} + 54.32$) is presented with estimation of hysteresis time by discharge rate. These results may be helpful for designing and precise controlling of a similar battery module cooling system.

In the future, based on this study, more useful work can be done about how to design an efficient BTMS considering the real situation that transient thermal regimes vary a lot because of a large number of operating conditions. And transient experiments and simulations of battery pack with different cooling systems are worth doing to find different transient and ultimate thermal characteristics, which will greatly improve the current BTMS for energy saving and intelligent control.

Acknowledgement

The research project has been funded by the National Science Foundation of China (Grant number 91741203). The authors would also like to appreciate the support by Royal Academy of Engineering through the Transforming Systems through Partnerships program (Grant number TSP1098) and the Newton Fund Innovation Partnership (Grant number 201703780098).

References

[1] Z. An, L. Jia, Y. Ding, C. Dang, X. Li, A review on lithium-ion power battery thermal management technologies and thermal safety, -Journal of Thermal Science, 26 (2017) 391-412.

[2] S. Hardman, E. Shiu, R. Steinberger-Wilckens, Changing the fate of Fuel Cell Vehicles: Can lessons be learnt from Tesla Motors?, International Journal of Hydrogen Energy, 40 (2015) 1625-1638.

[3] L. Jin, P. Lee, X. Kong, Y. Fan, S. Chou, Ultra-thin minichannel LCP for EV battery thermal management, Applied Energy, 113 (2014) 1786-1794.

[4] W. Wu, W. Wu, S. Wang, K. Chen, S. Hong, Y. Lai, A critical review of battery thermal performance and liquid based battery thermal management, Energy Conversion and Management, 182 (2019) 262-281.

[5] T. Deng, G. Zhang, Y. Ran, P. Liu, Thermal performance of lithium ion battery pack by using cold plate, Applied Thermal Engineering, 160 (2019) 114088.

[6] Z. Rao, X. Zhang, Investigation on thermal management performance of wedge-shaped microchannels for rectangular Li-ion batteries, International Journal of Energy Reasarch, 43 (2019) 3876-3890.

[7] Y. Wang, G. Zhang, X. Yang, Optimization of liquid cooling technology for cylindrical power battery module, Applied Thermal Engineering, 162 (2019) 114200.

[8] Y. Huo, Z. Rao, X. Liu, J. Zhao, Investigation of power battery thermal management by using mini-channel cold plate, Energy Conversion and Management, 89 (2015) 387-395.

[9] A. Tang, J. Li, L. Lou, C. Shan, X. Yuan, Optimization design and numerical study on water cooling structure for power lithium battery pack, Applied Thermal Engineering, 159 (2019) 113760.

[10] O. Yetik, T.H. Karakoc, A numerical study on the thermal performance of prismatic li-ion batteries for hibrid electric aircraft, Energy, 195 (2020) 117009.

[11] Y. Alkhulaifi, N. Qasem, S. Zubair, Improving the performance of thermal management system for electric and hybrid electric vehicles by adding an ejector, Energy Conversion and Management, 201 (2019) 112133.

[12] H.S. Hamut, I. Dincer, G.F. Naterer, Analysis and optimization of hybrid electric vehicle thermal management systems, Journal of Power Sources, 247 (2014) 643-654.

[13] X. Gao, Y. Ma, H. Chen, Active thermal control of a battery pack under elevated temperatures, International Feferation of Automatic Control, 51 (2018) 262-267.

[14] Y. Liu, J. Zhang, Self-adapting J-type air-based battery thermal management system via model

predictive control, Applied Energy, 263 (2020) 114640.
[15] Y. Hu, H. Chen, H. Chen, P. Wang, L. Ren, Nonlinear model predictive controller design based on learning model for turbocharged gasoline engine of passenger vehicle, Mechanical Systems and Signal Processing, 109 (2018) 74-88.
[16] M. Al-Zareer, I. Dincer, M.A. Rosen, Novel thermal management system using boiling cooling for high-powered lithium-ion battery packs for hybrid electric vehicles, Journal of Power Sources, 363 (2017) 291-303.
[17] D. Kong, R. Peng, P. Ping, J. Du, G. Chen, J. Wen, A novel battery thermal management system coupling with PCM and optimized controllable liquid cooling for different ambient temperatures, Energy Conversion and Management, 204 (2020) 112280.
[18] T. Deng, Y. Ran, Y. Yin, P. Liu, Multi-objective optimization design of thermal management system for lithium-ion battery pack based on Non-dominated Sorting Genetic Algorithm II, Applied Thermal Engineering, 164 (2020) 114394.
[19] Y. Fan, Y. Bao, C. Ling, Y. Chu, X. Tan, S. Yang, Experimental study on the thermal management performance of air cooling for high energy density cylindrical lithium-ion batteries, Applied Thermal Engineering, 155 (2019) 96-109.
[20] D. Bernardi, D. Bernardi, E. Pawlikowski, E. Pawlikowski, J. Newman, J. Newman, General energy balance for battery systems, Journal of the Electrochemical Society, 132 (1985) 5-12.
[21] Y. Huang, Y. Lu, R. Huang, J. Chen, F. Chen, Z. Liu, X. Yu, A.P. Roskilly, Study on the thermal interaction and heat dissipation of cylindrical Lithium-Ion Battery cells, Energy Procedia, 142 (2017) 4029-4036.